Enhancing Bandwidth and Back-Off Range of Doherty Power Amplifier With Modified Load Modulation Network

Yang Xu, *Graduate Student Member, IEEE,* Jingzhou Pang, *Member, IEEE,*
Xiaoyu Wang, *Graduate Student Member, IEEE* and Anding Zhu, *Senior Member, IEEE*

***Abstract*—This paper presents a novel methodology for designing broadband Doherty power amplifier (DPA) with extended output power back-off (OBO) range. A modified load modulation network (LMN) is proposed to enhance the OBO range and the bandwidth of the DPA simultaneously. Analysis is conducted to explore the relationship between the proposed LMN parameters and the broadband performance under various OBO levels. Generalized design formulas of the LMN parameters are then introduced to offer the broadband solution for arbitrary current ratios and OBO levels. An asymmetric DPA is demonstrated and implemented with Gallium Nitride (GaN) transistors using the proposed approach. The fabricated DPA operates from 1.4 GHz to 2.5 GHz with 9-dB OBO range. The measured drain efficiency reaches 61%-75.5% at saturation and 44.6%-54.6% at 9-dB OBO within the operating bandwidth. When driven by a 60 MHz modulated signal with 9-dB peak-to-average power ratio (PAPR), the fabricated DPA attains 47.4%-53.5% average drain efficiency and better than -45.5 dBc adjacent channel leakage ratio (ACLR) after digital predistortion.**

***Index Terms*—5G, broadband, Doherty amplifier, GaN, load modulation, power amplifier.**

I. Introduction

With the rapid development of modern wireless communication systems, dramatic increase in data traffic poses significant challenges on implementing radio frequency (RF) power amplifiers (PAs) in wireless transmitters. On one hand, the growing traffic and data rates demand the PAs to support wide signal bandwidth. On the other hand, to improve spectrum efficiency, modulated signals with high peak-to-average power ratio (PAPR) are commonly adopted that require the PAs to provide high efficiency performance not only at saturation but also at output power back-off (OBO). It is thus desirable to have PA architectures that can achieve high OBO efficiency cross broad bandwidth. This desire becomes imminent in the 5G era, since the signal bandwidth is expected to be extended to hundreds of MHz and a variety of higher order modulation schemes leads to different OBO levels.

This work was supported in part by the Science Foundation Ireland under Grant Numbers 13/RC/2077, 17/NSFC/4850 and 16/IA/4449. (*Corresponding author: Jingzhou Pang*)

Y. Xu, X. Wang and A. Zhu are with the School of Electrical and Electronic Engineering, University College Dublin, Dublin 4, Ireland (e-mail: yang.xu@ucdconnect.ie; xiaoyu.wang1@ucdconnect.ie; anding.zhu@ucd.ie).

J. Pang was with the School of Electrical and Electronic Engineering, University College Dublin, Dublin 4, Ireland and now is with the School of Microelectronics and Communication Engineering, Chongqing University, 400044 Chongqing, China (e-mail: jingzhou.pang@cqu.edu.cn).

In past decades, many techniques and architectures, such as Doherty power amplifier (DPA), out-phasing and envelope tracking, have been proposed to improve the PA efficiency performance at OBO. Among them, DPA has become one of the most popular techniques for OBO efficiency enhancement because of its simple circuit structure and high reliability. However, the conventional DPA that adopts a quarter-wavelength transmission line (TL) as the load modulation network (LMN) is intrinsically narrow band, and the power back-off level that the conventional DPA can offer is limited. To improve the efficiency when transmitting high PAPR modulated signals, the asymmetric DPA architectures can be deployed to extend the OBO range. To realize the asymmetric DPAs, active devices with different sizes [1]–[3], or asymmetric supply voltage [4], [5] can be adopted. In these asymmetric DPA architectures, a larger size active device or a higher drain bias voltage are used in the peaking PAs to ensure higher peaking output power. Unlike these asymmetric DPAs, for the DPAs utilizing the equal-cell devices, the OBO range can also be enhanced through modifying the current combining strategy between the carrier and the peaking PAs [6]–[8]. It should be noticed that, as the LMNs of the above mentioned DPAs usually require higher impedance transformation ratio, it is thus difficult for them to maintain high performance cross wide bandwidth.

Since the bandwidth limitation is mainly caused by the frequency dependent behavior of the quarter-wavelength TL, lots of efforts have been made to obtain wider bandwidth by modifying the LMN architecture in DPA [9]–[12]. The impact from the matching network of the peaking amplifier on bandwidth was also discussed in [13], [14]. It has been shown that, when a half-wavelength TL or two quarter-wavelength TLs with different characteristic impedances are employed in the peaking branch, the bandwidth of DPAs can be greatly extended [15]–[17]. By employing other techniques such as using the complex load [18], [19], adding a stub at the combining node [20], [21], optimizing the post-matching architecture [22], [23], adopting the continuous mode theory [24], [25] and exploring the phase characteristics of the LMNs [26]–[28], the bandwidth of DPAs can also be extended. Despite efforts were made, these bandwidth extension techniques mainly focus on DPAs with 6-dB OBO. When considering the DPAs with larger OBO ranges, the designs become much more complex. This is because that, the available OBO is decided by the LMN structure and the corresponding design parameters. Even under the same OBO level, the presented bandwidth performance

varies with the LMN design. Therefore, the bandwidth extension technique under a specific OBO level might not be applicable to the design at other different OBO levels.

To enhance the OBO range and the bandwidth simultaneously, some efforts have been made by combining the above mentioned techniques together [29]–[33]. In these approaches, the desired OBO is usually given at the first step and the LMN is modified to deliver the satisfied bandwidth performance. The impedance analysis is then conducted to search for the optimal LMN and the corresponding current relationship between the carrier and the peaking amplifiers. Although these efforts provide practicable methods to design DPAs with both enhanced OBO range and bandwidth, the bandwidth performance still depends on the specific LMN structure and design parameters. The optimal current combining strategy or the optimal LMN structure might be only suitable for the designed OBO. At different OBO levels, the LMN should be re-designed and the optimal parameters must be re-chosen. Thus, it is difficult to transplant the LMN design directly to other OBO levels and the bandwidth performance can not be guaranteed. Very few studies have explored the relationship between the bandwidth and OBO range and it is also not clear how the LMN parameters affect the DPA performance.

In this paper, we propose a generalized approach to constructing the LMN for broadband DPAs operated at extended OBO levels. The modified LMN is simple to implement. The OBO and bandwidth performance of the DPA can be improved simultaneously by employing this LMN. This network is composed of several segments of TLs with different characteristic impedances. With the proposed LMN, case studies that ranging from symmetric to asymmetric structures under various scenarios are conducted, and the impact of LMN parameters on bandwidth with respect to the current ratio and the OBO level is also investigated. Based on these analysis, a series of generalized formulas for constructing the modified LMN are proposed, that facilitates the designers to build the DPA with high efficiency performance at an extended OBO level cross a wide bandwidth. Unlike other reported designs, the proposed formulas cover a wide range of OBO and broadband characteristics at these OBO levels can be obtained with the proposed approach. Moreover, the analysis made under different scenarios reveals the relationship between the LMN parameters and the DPA performance. An asymmetric DPA with 9-dB OBO range is prototyped to demonstrate the design procedure.

The rest of the paper is organized as follows. The design principle of the proposed DPA and case studies are given in Section II with generalized design formulas for the modified LMN. In Section III, an asymmetric prototype DPA is designed based on the optimal LMN parameters suggested by proposed formulas to validate the design approach. The measured performance of the fabricated DPA is presented in Section IV with a conclusion in Section V.

II. The Design Principle

As shown in Fig. 1(a), in a conventional DPA, a quarter-wavelength TL with characteristic impedance of R_{opt} that is

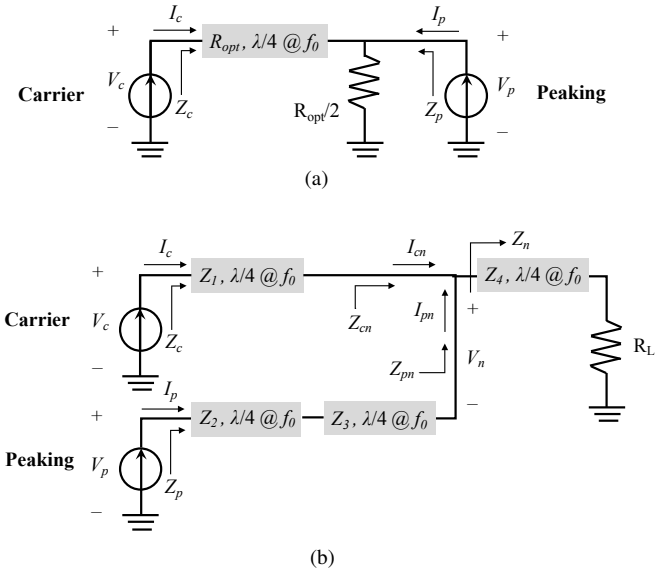

(a)

(b)

Fig. 1. Block diagram of the (a) conventional DPA (b) DPA with modified LMN.

the optimal impedance of the carrier amplifier, is used as the LMN. In this design, the bandwidth of the DPA is intrinsically narrow due to the frequency dependent characteristic of the quarter-wavelength TL. The OBO level is dependent on the current ratio of the carrier amplifier over the peaking amplifier. In a symmetric design, high efficiency only can be achieved at 6 dB OBO since the LMN transfers the load $R_L = R_{opt}/2$ to $2R_{opt}$ at 6-dB OBO. To meet different design criterion, the LMN must be modified and its circuit parameters shall be adjusted accordingly.

The preliminary study in [34] shows, for the LMN that consists of several segments of TLs, by modifying the characteristic impedance of these TLs, the high efficiency range and the bandwidth performance of the DPA can be improved. In this work, we further modify the LMN and propose a general network structure as shown in Fig. 1(b), where four quarter-wavelength TLs are used and $Z_i (i = 1, 2, 3, 4)$ represents the characteristic impedance of each TL, respectively.

The modified LMN includes multiple segments of TLs with changeable characteristic impedance for each segment, which greatly extends the design space and makes it possible to accommodate varies settings of the current ratios and OBO levels required by the DPAs, including both symmetric and asymmetric architectures. In following subsections, we will discuss how the LMN parameters can be chosen according to the OBO and bandwidth requirements in DPA design. Firstly, the characteristic impedance relationship of the employed TLs at the center operating frequency is given, and based on this, the in-phase combining condition is applied to search for LMN parameters that satisfy the required phase relationship between the carrier and peaking amplifiers when considering the broadband operation. Because of the complexity of the phase relations, direct analytical solutions are hard to find. Alternatively, cases studies under different operating settings are discussed. Finally, a series of generalized design formulas for determining the LMN parameters are given by using data

fitting.

A. Characteristic Impedance Relationship

For convenience of analysis, the carrier and peaking active devices are regarded as ideal voltage-controlled current generators (CGs) in the following discussion. Let's assume all the employed TLs have electrical length equal to 90° at the center operating frequency f_0. At OBO, the impedances at the CG planes can be calculated as,

$$Z_{c,obo\_f_0} = \frac{Z_1^2}{Z_4^2} R_L, \tag{1}$$

$$Z_{p,obo\_f_0} = \infty. \tag{2}$$

where Z_{c,obo_f_0} and Z_{p,obo_f_0} represents the impedance of the carrier and the peaking amplifier, respectively. When the DPA is saturated, the maximum current of the carrier and the peaking amplifier is defined as $I_{c,max}$ and $I_{p,max}$, respectively. The current ratio of the carrier amplifier over the peaking amplifier can then be defined as $\alpha = I_{p,max}/I_{c,max}$. The impedances at saturation can be calculated as,

$$Z_{c,sat\_f_0} = \frac{Z_1^2}{Z_4^2} R_L - \frac{Z_1 Z_2}{Z_3}\alpha, \tag{3}$$

$$Z_{p,sat\_f_0} = \frac{Z_1 Z_2}{Z_3 \alpha}. \tag{4}$$

where Z_{c,sat_f_0} and Z_{p,sat_f_0} denotes the impedance at the carrier and peaking CG plane, respectively, when the DPA is saturated.

With those impedances, the OBO level β can be expressed as,

$$\beta = \sqrt{\frac{(I_{c,max} Z_{c,sat\_f_0})^2 / Z_{c,obo\_f_0}}{I_{c,max}^2 Z_{c,sat\_f_0} + I_{p,max}^2 Z_{p,sat\_f_0}}}. \tag{5}$$

When expressed in dB scale, we have $OBO = -20log_{10}(\beta)$. By substituting (1)(3)(4) into (5), the carrier impedance at OBO can be expressed as,

$$Z_{c,obo\_f_0} = \frac{1}{\beta} Z_{c,sat\_f_0}. \tag{6}$$

By substituting (3)(4) into (6), the peaking impedance at saturation can also be written as,

$$Z_{p,sat\_f_0} = \frac{1}{\alpha^2}(\frac{1}{\beta} - 1) Z_{c,sat\_f_0}. \tag{7}$$

The equations above reveal that the impedances are defined with respect to the OBO level β and the current ratio α. With different α and β, the impedances Z_{c,obo_f_0}, Z_{c,sat_f_0} and Z_{p,sat_f_0} vary with them, consequently, determine the selection of TL characteristic impedances. For instance, in the conventional symmetric DPA with 6-dB OBO, $\alpha = 1$ and $\beta = 1/2$, and $Z_{p,sat\_f_0} = Z_{c,sat\_f_0}$, $Z_{c,obo\_f_0} = 2Z_{c,sat\_f_0}$. For the proposed LMN, there are five LMN parameters, namely, Z_1, Z_2, Z_3, Z_4 and R_L. They can be chosen according to the defined the impedance relationship obtained. Among the five parameters, three independent parameters can be chosen freely according to the given impedance relationships, and the rest two parameters can be obtained based on (1)(3)(4). If we let Z_1, Z_2 and R_L be the independent parameters, the characteristic impedances Z_3 and Z_4 can be then calculated as,

$$Z_3 = \frac{Z_1 Z_2 \alpha}{(\frac{1}{\beta} - 1) R_{opt}}, \tag{8}$$

$$Z_4 = Z_1 \sqrt{\frac{\beta R_L}{R_{opt}}}. \tag{9}$$

Because of the three degrees of freedom, with a given current ratio and OBO level, there are more than one feasible configuration of Z_i and R_L that can provide the proper load modulation at the center frequency. When it comes to the broadband operation, the selection of the independent parameters can be used to explore the impact on the bandwidth under the proposed modified LMN.

B. Broadband Operation Based on In-Phase Combining

The bandwidth performance of the modified LMN varies with the α and β, and is determined by the current combining strategy, especially for the asymmetric architecture. The current relationship at the combing node relates to the selection of LMN parameters. As shown in Fig. 1(b), the current at the carrier branch is I_{cn} and the current at the peaking branch is I_{pn}. The relationship between I_{cn} and I_{pn} can be expressed as,

$$I_{cn} = \frac{I_c - j \sin\theta \frac{Z_n}{Z_1} I_{pn}}{\cos\theta + j \sin\theta \frac{Z_n}{Z_1}}. \tag{10}$$

Similarly, for the peaking amplifier, the following relationship can be obtained,

$$I_{pn} = \frac{I_p - j \frac{\sin 2\theta}{2}(\frac{1}{Z_2} + \frac{1}{Z_3}) Z_n I_{cn}}{\cos^2\theta - \frac{Z_3}{Z_2}\sin^2\theta + j\frac{\sin 2\theta}{2}(\frac{1}{Z_2} + \frac{1}{Z_3}) Z_n} \tag{11}$$

where Z_n denotes the impedance at the combining node, and can be written as,

$$Z_n = Z_4 \frac{R_L + jZ_4 \tan\theta}{Z_4 + jR_L \tan\theta}, \tag{12}$$

where θ represents the phase delay of the quarter-wavelength TL. It can be expressed as $\theta = (\pi/2)f$, where f is the operating frequency normalized to the center frequency f_0.

The way how I_{cn} and I_{pn} are combined across the operating frequency would affect the bandwidth performance. For the modified LMN, the current relationship at the combining node becomes complex because of multiple segments of TLs involved. The magnitudes of I_{cn} and I_{pn} vary with frequency, and the phase dispersion of both currents might not be the same across the operating frequencies. Moreover, the characteristic impedances in (10)(11)(12) are independent parameters that also are related to the current ratio and the desired OBO level. Thus, it is difficult to determine the desired current combining mode analytically, especially when varying both current ratio and OBO levels. As an alternative, we assume that I_{cn} and I_{pn} have same behavior as the conventional DPA. To

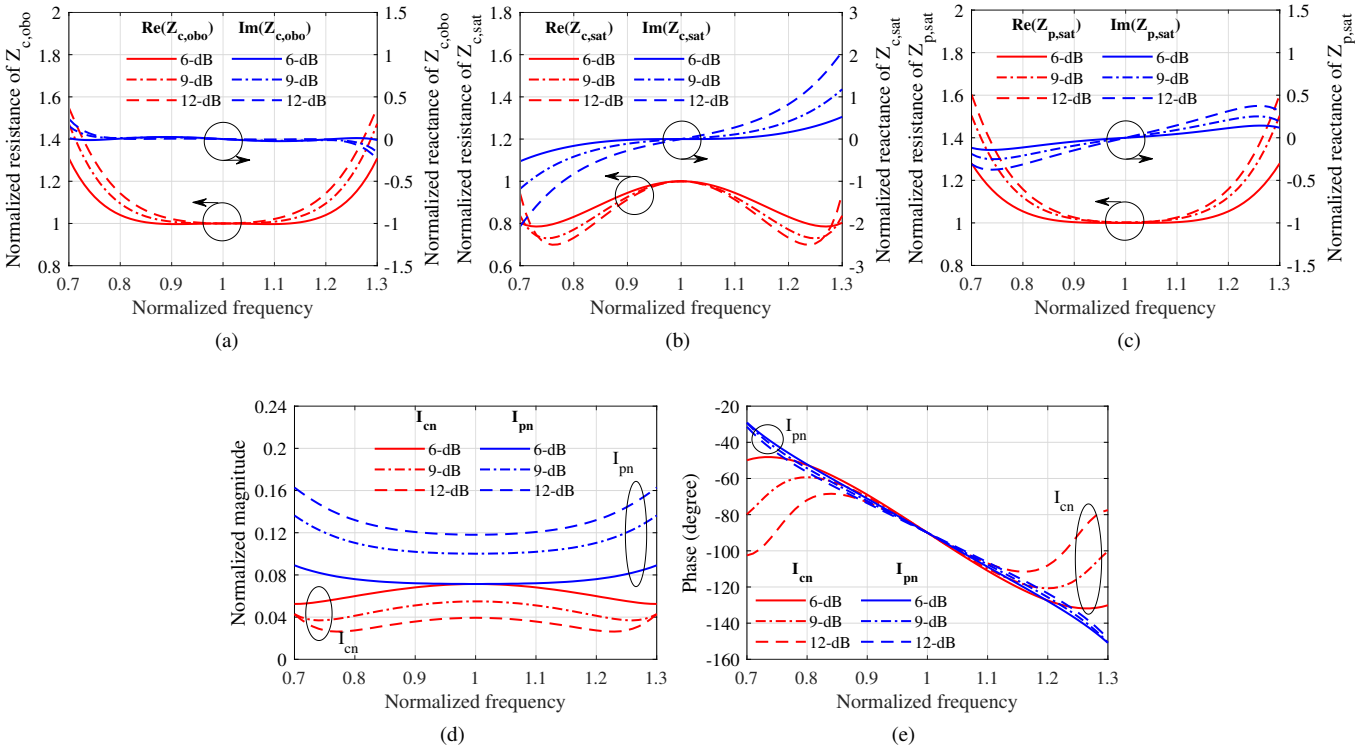

Fig. 2. Simulated impedances inside the bandwidth under the equal impedances at saturation (a) $Z_{c,obo}$ (b) $Z_{c,sat}$ (c) $Z_{p,sat}$. The current (d) magnitude and (e) phase of I_{cn} and I_{pn} at the combing node.

be more specific, I_{cn} and I_{pn} are expected to perform in-phase combining across the bandwidth with constant magnitude for all settings of α and β. The bandwidth performance is then investigated under this condition.

An assumption is made that the magnitude of I_{cn} and I_{pn} keep constant regardless of the frequency variation, and equal to their values at the center frequency f_0. The phase relationship complies with $\angle I_{cn} = \angle I_{pn}$, which guarantees I_{cn} and I_{pn} combined in phase at every frequency point. Based on this assumption, I_{cn} and I_{pn} can be expressed as,

$$I_{cn} = I_c \frac{R_{opt}}{Z_1} e^{j\theta_n}, \tag{13}$$

$$I_{pn} = I_c \alpha \frac{Z_2}{Z_3} e^{j\theta_n}, \tag{14}$$

where θ_n represents the phase of I_{cn} and I_{pn}. To ensure the correct load modulation process, the phase of I_c should be 90° delayed than I_p. When arriving the combing node, the phase delay is expected as

$$\theta_n = \frac{\pi}{2} - \pi f. \tag{15}$$

At saturation, the current relationship $I_{p,max} = \alpha I_{c,max} e^{j\pi f/2}$ should be satisfied. Substituting (13)(14) into (10) and (11) respectively, the following relationship can be obtained,

$$e^{j\theta_n} = \frac{Z_1}{R_{opt}(\cos\theta + j \sin\theta \frac{Z_n}{Z_1}\frac{1}{\beta})}, \tag{16}$$

$$\begin{aligned} e^{j(\theta-\theta_n)} = {} & \frac{Z_2}{Z_3}\cos^2\theta - \sin^2\theta \\ & + j\frac{\sin 2\theta}{2} Z_n \left(\frac{1}{Z_2} + \frac{1}{Z_3}\right)\frac{Z_2}{Z_3}\frac{1}{1-\beta}. \end{aligned} \tag{17}$$

Under a given α and β, if LMN design parameters satisfy (16)(17), I_{cn} and I_{pn} are able to combine in phase inside the operating frequency band with constant magnitude. As analyzed, there are three independent parameters that can be used to explore the bandwidth performance. The LMN design parameters can be attained by solving the conditions applied. However, this requires complex mathematical calculations, and the obtained equivalent characteristic impedances would be frequency-dependent, which may not be always possible to implement in real practice. Instead, if we can find the independent parameters that has real constant numbers and fit the equations to the greatest extend, they can be considered as the desired solutions for the proposed modified LMN.

C. Case Studies

The modified LMN is capable of accommodating the flexible configurations of α and β. While α and β are relatively independent from each other, when selecting different settings of α and β, the optimal LMN parameters that satisfy the assumption would vary. To investigate the impact individually, case studies under different scenarios are conducted. Each case corresponds to a certain relationship between α and β. In each scenario, the configuration parameters of α and β

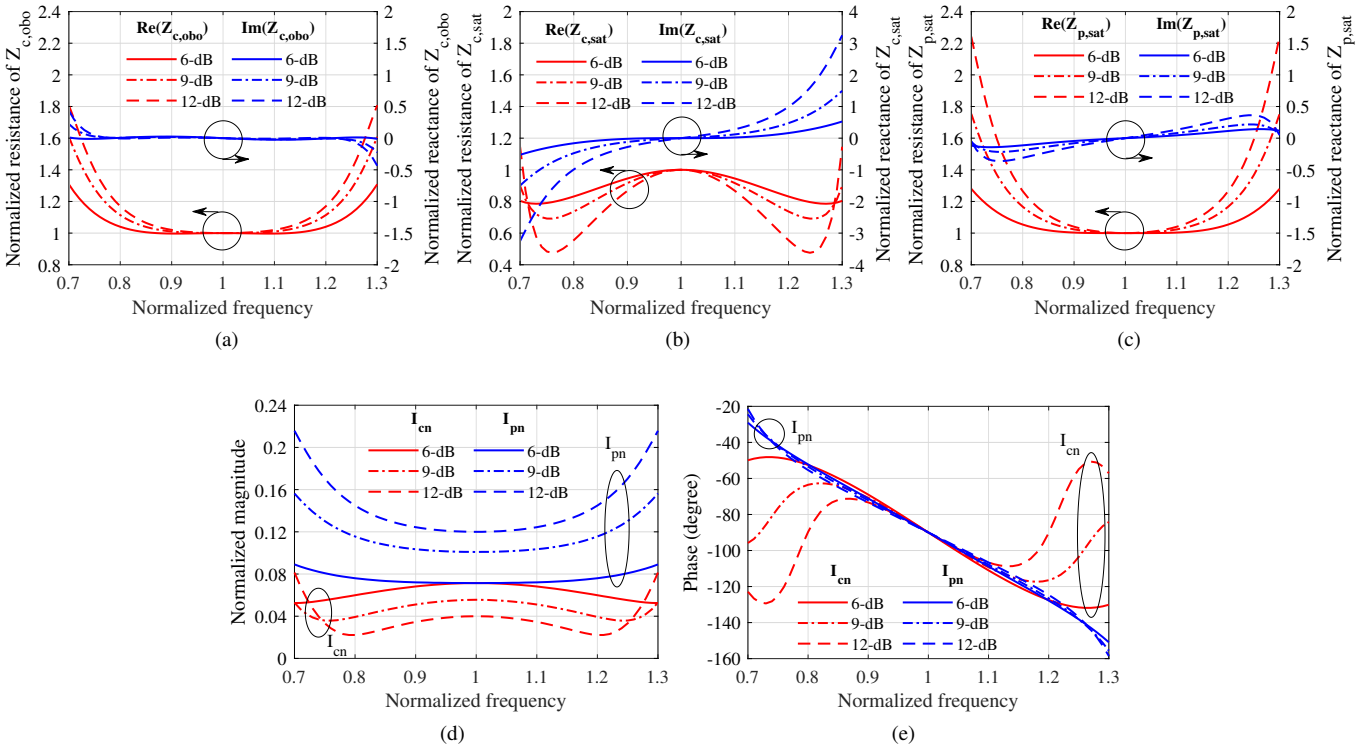

Fig. 3. Simulated impedances inside the bandwidth under the equal current level (a) $Z_{c,obo}$ (b) $Z_{c,sat}$ (c) $Z_{p,sat}$. The current (d) magnitude and (e) phase of I_{cn} and I_{pn} at the combing node.

are given as the precondition and then, the LMN parameters are obtained by evaluating the bandwidth performance. With the data collected from various scenarios, the generalized broadband solution of LMN parameters can be obtained by using data fitting.

The carrier impedance at OBO $Z_{c,obo}$, the saturated impedances $Z_{c,sat}$ and $Z_{p,sat}$ are simulated to evaluate the broadband performance. As discussed earlier, when α and β are fixed, there are three independent parameters for the proposed LMN. The characteristic impedance of the TLs can be tuned to search for the combination of Z_i and R_L that agrees with the relationship described by (16)(17) most. According to (9), Z_4 relates to β and R_L, and parameters involved in (16) are β, Z_1 and R_L. This means, at a given OBO level, Z_1 and R_L are defined by this relationship regardless of the current ratio α. Under a given current ratio α, Z_2 can be adjusted to satisfy (17). Once independent parameters Z_1, Z_2 and R_L are found, Z_3 and Z_4 can be calculated from (8)(9) subsequently.

1) Case I: Equal Impedances at Saturation: The first case is that the carrier and peaking CGs have the same optimal impedance at saturation, namely $Z_{c,sat} = Z_{p,sat} = R_{opt}$. Consequently, the relationship $\alpha^2 = 1/\beta - 1$ can be conducted according to (7).

With different OBO levels, the current ratio changes accordingly, independent parameters Z_1, Z_2 and R_L are tuned to fit conditions applied in (16)(17). Simulated results under 6-/9-/12-dB OBO are shown in Fig. 2, where the simulated impedances $Z_{c,obo}$, $Z_{c,sat}$ and $Z_{p,sat}$ are normalized to their

TABLE I
THE TUNED CHARACTERISTIC IMPEDANCES UNDER THE EQUAL IMPEDANCES AT SATURATION

OBO	α	Z_{c,obo_f_0}	Z_1	Z_2	Z_3	Z_4	R_L
6 dB	1	2	1.4	1.14	1.6	1.29	1.7
9 dB	1.35	2.82	1.8	1.2	1.6	1.52	2
12 dB	1.73	4	2.5	1.34	1.93	2.01	2.6

values at the center frequency for better presentation. The optimal values of Z_i and R_L, which have been normalized to the optimal impedance R_{opt}, are summarized in Table I. At OBO, the resistance of $Z_{c,obo}$ has larger variation when the OBO level increases, while the reactance is almost constant across the bandwidth of interest. At saturation, larger variation of $Z_{c,sat}$ and $Z_{p,sat}$ can be observed at higher OBO level. The resistance of $Z_{c,sat}$ shows more steady performance compared to its reactance. Whereas for $Z_{p,sat}$, the reactance of it maintains a relatively flat frequency response compared to the resistance. With increasing OBO level, the magnitude of I_{pn} alters more than that of I_{cn} inside the bandwidth. But it is the opposite with respect to the phase, $\angle I_{pn}$ sticks to the expected θ_n while $\angle I_{cn}$ differs from it as the frequency deviating from the center frequency.

2) Case II: Equal Current Level: The second case analysed is the DPA in which the saturated current levels of two active devices equal to each other. In this situation, for a given OBO level, the current ratio remains constant, and

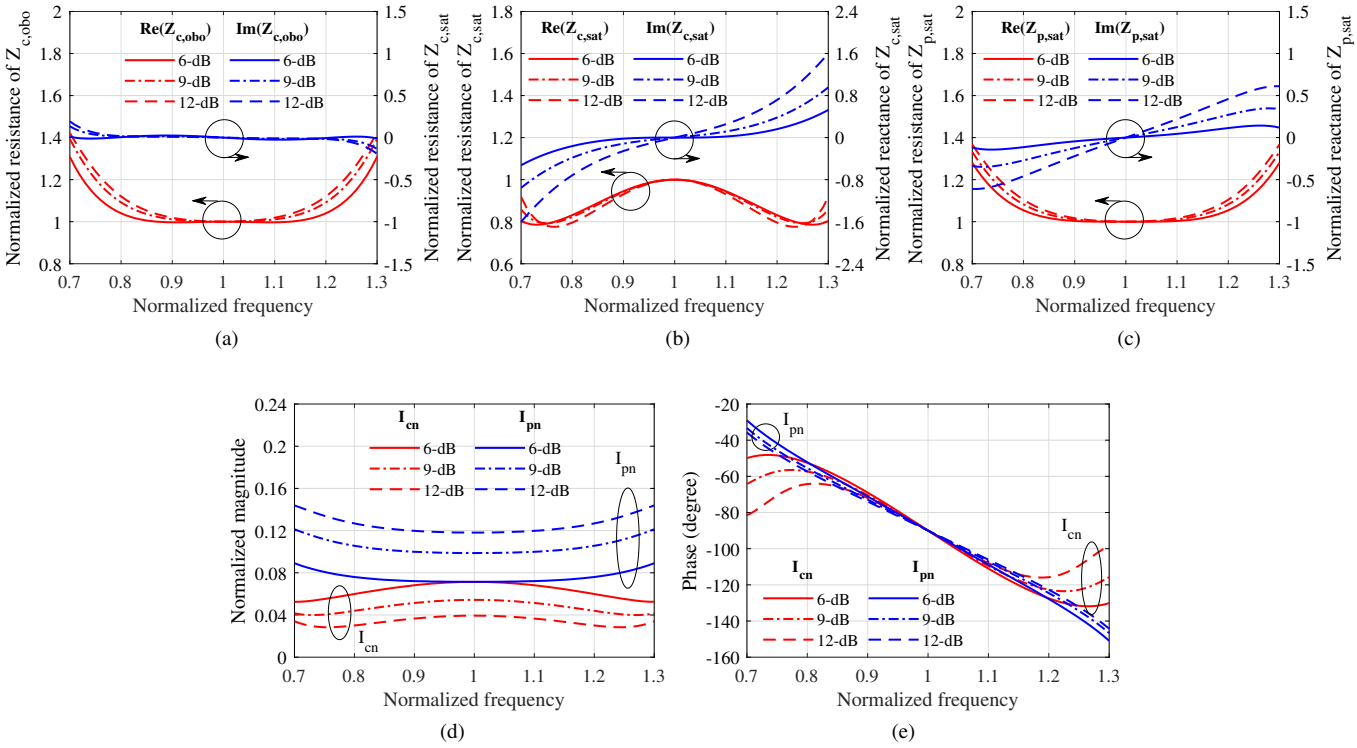

Fig. 4. Simulated impedances inside the bandwidth under the equal supply voltage (a) $Z_{c,obo}$ (b) $Z_{c,sat}$ (c) $Z_{p,sat}$. The current (d) magnitude and (e) phase of I_{cn} and I_{pn} at the combing node.

we can simply obtain $\alpha = 1$. At the center frequency, the saturated impedance of the peaking amplifier when referring to the carrier optimal impedance R_{opt} can be expressed as $Z_{p,sat\_f_0} = (1/\beta - 1)R_{opt}$. Similarly, Z_1, Z_2 and R_L are tuned to search for the optimal broadband solution. The simulated impedance results under 6-/9-/12-dB OBO are shown in Fig. 3 and the obtained characteristic impedances Z_i and R_L are summarized in Table. II. Since Z_{c,obo_f_0} only depends on β which is the same as the previous case discussed, its value is not repeated in this table.

The 6-dB OBO case is the same as the previous one since the equal current level and the equal saturated impedance happen at the same time. With a larger OBO level, the increase of $Z_{c,obo}$ resistance is slightly bigger than that in the last case discussed, the reactance still maintains almost constant across wide bandwidth. At saturation, behaviours of $Z_{c,sat}$ and $Z_{p,sat}$ are similar with that in the case of equal impedances at saturation, but the fluctuation inside the bandwidth is relatively larger. The magnitude and phase of I_{cn} and I_{pn} increase sharply with large OBO level. Due to the large variation, the available bandwidth is reduced.

3) Case III: Equal Supply Voltage: The third case is when the carrier and peaking CGs have the same drain supply voltage which is quite common in practice. The drain supply voltage adopts the maximum fundamental voltage reached at saturation, which is represented by $V_{c,max}$ for the carrier amplifier and $V_{p,max}$ for the peaking amplifier. Based on (7),

TABLE II
THE TUNED CHARACTERISTIC IMPEDANCES UNDER THE EQUAL CURRENT LEVEL

OBO	Z_{p,sat_f_0}	Z_1	Z_2	Z_3	Z_4	R_L
6 dB	1	1.4	1.14	1.6	1.29	1.7
9 dB	1.82	1.8	1.82	1.8	1.51	1.98
12 dB	3	2.46	2.88	2.36	1.98	2.6

when considering the drain supply voltage we have

$$V_{p,max} = \frac{1}{\alpha}(\frac{1}{\beta} - 1)V_{c,max} \tag{18}$$

Thus, the relationship between α and β can be conducted as $\alpha = 1/\beta - 1$ when $V_{c,max} = V_{p,max}$. The saturated impedance of the peaking amplifier at the center frequency can be written as $Z_{p,sat\_f_0} = R_{opt}/\alpha$. With 6-/9-/12-dB OBO, the independent parameters Z_1, Z_2 and R_L are tuned for the optimal broadband performance. Fig. 4 presents the simulated impedance performance, and the optimal characteristic impedances Z_i and R_L are summarized in Table. III. The impedance Z_{c,obo_f_0} remains the same under the discussed OBO, and is not repeated in this table.

The 6-dB OBO case is the same as previous cases since the drain supply voltage is the same for both PAs. At OBO, the impedance variation of $Z_{c,obo}$ between different OBO levels is reduced than the previous two cases. At saturation, the real part variation of $Z_{c,sat}$ and $Z_{p,sat}$ is also smaller compared to the imaginary part. Similarly for the currents I_{cn} and I_{pn}

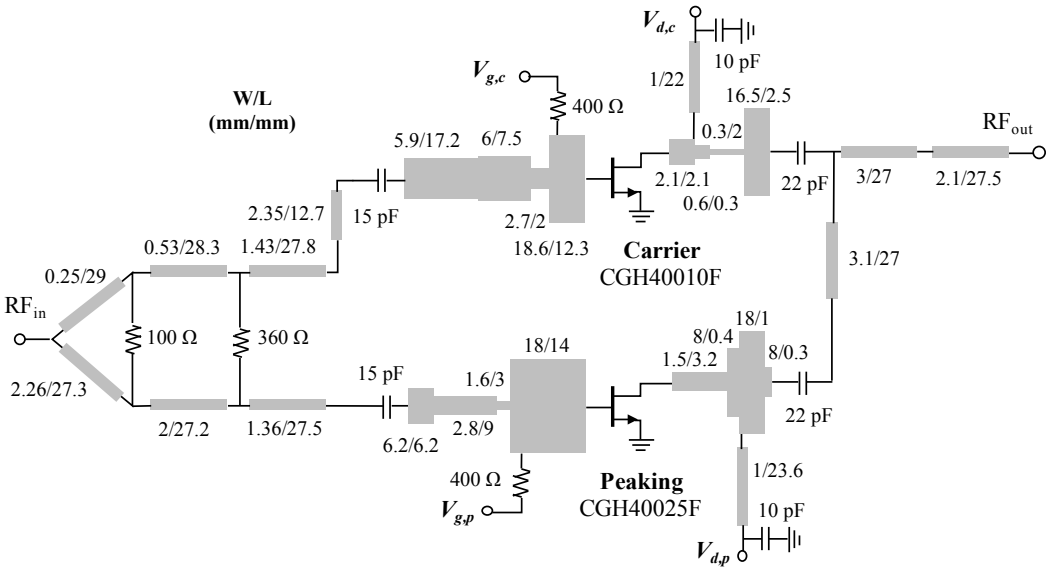

Fig. 5. Circuit schematic of the proposed DPA.

TABLE III
THE TUNED CHARACTERISTIC IMPEDANCES UNDER THE EQUAL SUPPLY VOLTAGE

OBO	α	Z_{p,sat_f_0}	Z_1	Z_2	Z_3	Z_4	R_L
6 dB	1	1	1.4	1.14	1.6	1.29	1.7
9 dB	1.82	0.55	1.8	0.82	1.47	1.52	2
12 dB	3	0.33	2.5	0.64	1.6	2.02	2.6

TABLE IV
CALCULATED CHARACTERISTIC IMPEDANCES BASED ON PROPOSED FORMULAS

OBO	α	Z_1	Z_2	Z_3	Z_4	R_L
6 dB	1	1.414	1.148	1.624	1.307	1.707
9 dB	1	1.79	1.836	1.812	1.515	2.012
	1.35		1.206	1.607		
	1.82		0.796	1.423		
12 dB	1	2.482	2.87	2.37	1.991	2.576
	1.73		1.33	1.906		
	3		0.616	1.53		

at the combining node, the fluctuation of the magnitudes is reduced, and the phases agree with the expected θ_n at wider bandwidth.

D. Generalized Design Formulas

Through assigning different combinations of α and β in the case studies, the impact of LMN parameters on broadband performance is clear now. The simulation results show that, inside the investigated bandwidth, the modified LMN can provide relatively flat impedance performance at OBO for all cases. The saturated impedances vary from case to case, but its deviation from optimal values can be controlled within a certain range. In contrast to the conventional symmetric DPA, the asymmetric current offers broader bandwidth and it can help to extend the back-off level simultaneously. The bandwidth performance is better in the scenarios with larger current ratio α. Moreover, with increasing OBO level, the bandwidth that can provide satisfied impedances also shrinks. Within the frequency region where I_{cn} and I_{pn} have relatively flat magnitude and synchronized phase, the impedances at OBO and saturation stick to the optimal value at f_0 better. Thus, how $\angle I_{cn}$ and $\angle I_{pn}$ follow θ_n can be used as the guideline for estimating the bandwidth.

Observing the simulated data under different scenarios, the TL characteristic impedance variation with the current level α and the OBO level β follows a certain pattern. When OBO is fixed, Z_1 and R_L maintain at a constant level, and that agrees with the assumption made in (16). Both of them increase with OBO level, and can be concluded as the function of β. While β is in inverse proportion to the OBO level, thus either its fraction $1/\beta$ or the element $1/\beta - 1$ appeared in (6) can be used to fit the function. Since the value increases with OBO at different gradients and are not linear, the exponent of β is adopted. Z_2 varies with both α and β, thus the fitting for it can be divided into two parts. Firstly, the fitting for β is conducted under the equal current level case where $\alpha = 1$. Then, the data for modeling the tendency of α can be extracted. With increasing α, Z_2 shows inversely proportion to it, similarly, the fraction $1/\alpha$ and the exponent of α are used to search for the corresponding fitting function.

From the characteristic impedance data under the discussed scenarios in Tables I, II and III, the following formulas can be used to calculate Z_1, Z_2 and R_L to meet the design requirements:

$$Z_1 = \frac{\sqrt{2}}{4\beta^2(\frac{1}{\beta}-1)^{\frac{3}{4}}} R_{opt}, \tag{19}$$

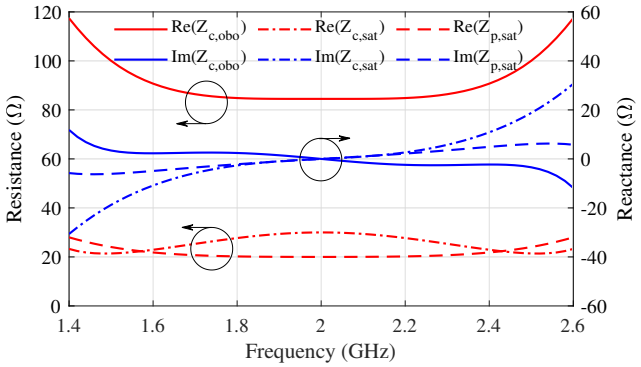

Fig. 6. Simulated impedance of the designed DPA at OBO and saturation based on proposed formulas.

$$Z_2 = \frac{1}{2\alpha^{1.4}} \frac{1}{\beta^{0.7}} (\frac{1}{\beta} - 1)^{\frac{1}{4}} \sqrt{\sqrt{\frac{1}{\beta} - 1} + 1} R_{opt}, \tag{20}$$

$$R_L = \frac{1}{\sqrt{2}} [\frac{1}{4} (\sqrt{\frac{1}{\beta} - 1} + \frac{1}{\sqrt{\frac{1}{\beta} - 1}})^2 + \frac{1}{2\beta^{\frac{3}{2}} \sqrt{\frac{1}{\beta} - 1}}] R_{opt}, \tag{21}$$

while Z_3 and Z_4 can be calculated by using (8)(9). To verify proposed formulas, the calculated results are presented in Table IV under the same α and β settings. It can be seen that, the calculated characteristic impedances agree well with the simulated results in all cases.

With the proposed formulas, the parameters of the LMN can be properly chosen in order to meet broadband performance for a wide range of α and β. The proposed formulas thus offer a generalized broadband solution to construct the LMN under an arbitrary current level α and OBO level β, including both symmetric and asymmetric DPA designs.

III. DPA Design

A prototype DPA was designed with Wolfspeed GaN HEMTs to validate the proposed design methodology and formulas. Based on the analysis, the asymmetric architecture with larger current ratio has better broadband performance. In this prototype, the CGH40010F transistor was selected for the carrier amplifier while the CGH40025F transistor was used for the peaking amplifier. The circuit was implemented on the Taconic TLY-5 substrate with dielectric constant of 2.2 and 30 mil thickness. The center operating frequency was set to 2.0 GHz. The circuit schematic of the DPA is shown in Fig. 5.

The carrier amplifier worked in Class-B mode, and the bias was chosen as $V_{g,c}$ = -3 V, $V_{d,c}$ = 28 V. Under this bias condition, the optimal impedance R_{opt} = 30 Ω at the intrinsic plane can be obtained according to the load-pull simulation, and the fundamental current magnitude can be estimated as 1.0 A at saturation. For the peaking amplifier, the drain supply voltage was adjusted to $V_{d,p}$ = 30 V, and α = 1.65 can be then expected. The gate bias was chosen at $V_{g,p}$ = -6 V. The saturated impedance for the peaking amplifier was calculated

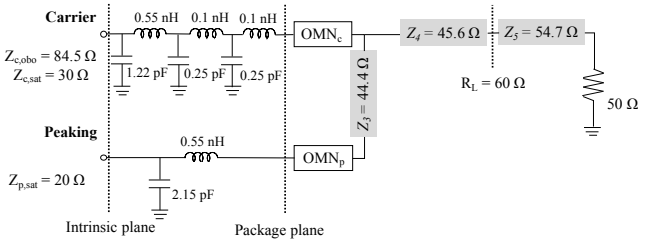

Fig. 7. The load modulation network of the DPA.

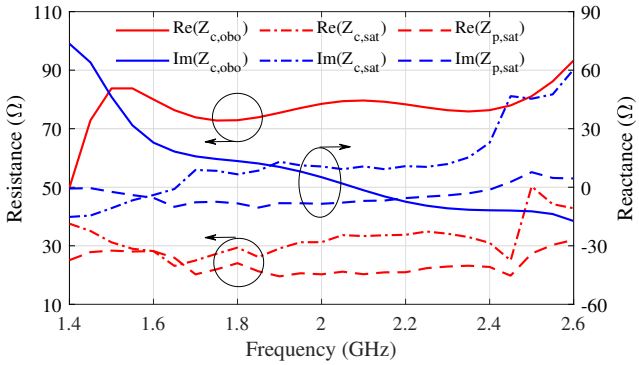

Fig. 8. Simulated impedances at the intrinsic plane at OBO and saturation of the proposed DPA.

as $Z_{p,sat}$ = 20 Ω at the intrinsic plane. According to (7), the expected OBO level can reach 9 dB. The LMN was designed according to the characteristic impedances calculated from (8)(9)(19)(20)(21), the values are Z_1 = $1.79R_{opt}$, Z_2 = $0.91R_{opt}$, Z_3 = $1.48R_{opt}$, Z_4 = $1.52R_{opt}$, R_L = $2R_{opt}$. The carrier impedance at OBO was estimated as Z_{c,obo_f_0} = 84.5 Ω.

With the proposed formulas, the calculated impedances for both amplifiers at OBO and saturation are illustrated in Fig. 6. At power back-off, the proposed LMN provides almost constant impedance inside 40% fractional bandwidth. $Z_{c,obo}$ increases a little with broader bandwidth, but still maintains at a satisfied level. When saturated, the real part of $Z_{c,sat}$ shows small variation inside 60% fractional bandwidth, whereas $Z_{p,sat}$ increases when deviating from the center frequency. The imaginary part of both $Z_{c,sat}$ and $Z_{p,sat}$ shows similar performance inside 40% fractional bandwidth, but $Z_{c,sat}$ rises more when extending to a wider bandwidth. Based on the analysis results, the bandwidth ranging from 1.4 GHz to 2.6 GHz can be achieved which corresponds to 60% fractional bandwidth.

In the analysis, Z_1 and Z_2 were connected to the CG planes directly. In practice, drain parasitic and package parameters need to be taken into consideration. Therefore, two matching networks absorbing the parasitic and package parameters were designed for both the carrier and peaking amplifiers as two equivalent quarter-wavelength TLs with characteristic impedance of Z_1 and Z_2, respectively. The extracted parasitic and package parameters of the carrier and peaking amplifier were obtained from [35] and [36] respectively. It should be noticed that the desired load was R_L = 60 Ω, thus a

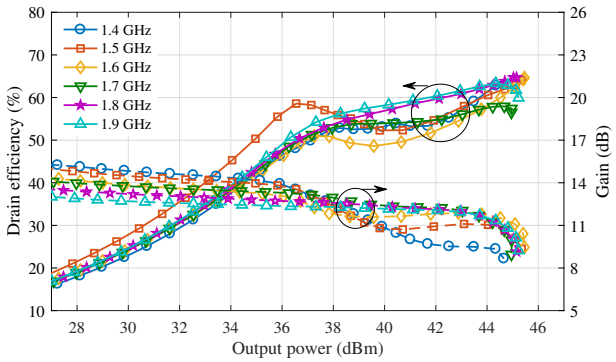

(a)

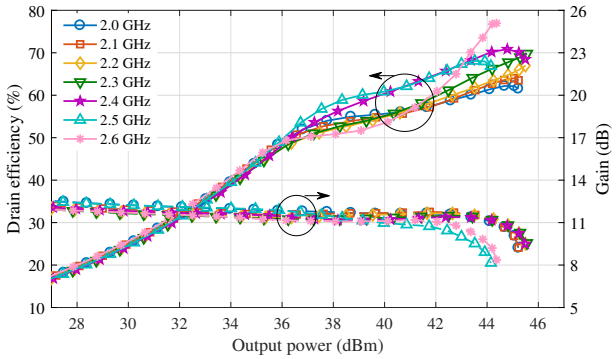

(b)

Fig. 9. Simulated drain efficiency and gain performance versus output power within the frequency range (a) 1.4-1.9 GHz and (b) 2.0-2.6 GHz.

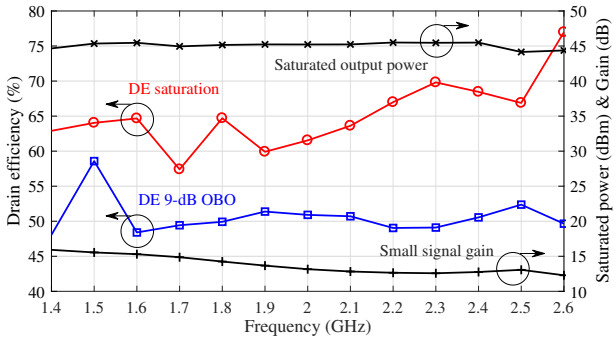

Fig. 10. Simulated drain efficiency at power saturation and 9-dB OBO, saturated power and small signal gain performance versus operating frequency.

matching network was added after Z_4 to transform R_L to the standard system load, which can be fulfilled by one quarter-wavelength TL with characteristic impedance Z_5. The entire LMN structure is shown in Fig. 7. With the launched LMN, the simulated impedances at OBO and saturation for both amplifiers at the intrinsic plane are presented in Fig. 8.

To provide the proper input power to both amplifiers, a broadband uneven Wilkinson power divider was designed and applied. The input power delivered to the carrier amplifier was $P_{in,c}$, and that of the peaking amplifier was $P_{in,p}$, the input power split ratio was $P_{in,p}$ - $P_{in,c}$ = 3.5 dB. The input matching network of each PA was designed according to the source-pull simulation which can provide broadband matching

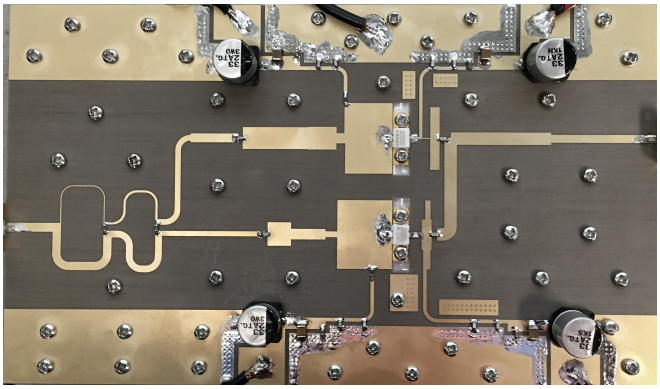

Fig. 11. Photograph of the fabricated DPA.

for both the carrier and the peaking amplifiers. A phase offset line was added before the input matching network of the carrier amplifier to assure the proper phase relationship. All design parameters were tuned for the optimized performance.

Power sweep simulation results within the operation bandwidth are presented in Fig. 9. It can be seen that the proposed PA achieves 9-dB OBO across the 60% fractional bandwidth. The drain efficiency maintains at a high level throughout the whole operating frequency band. To better present the simulated performance, frequency sweeping results are shown in Fig. 10. The maximum saturated output power reaches 45.5 dBm, and keeps above 44.2 dBm within the whole frequency range. The simulated small signal gain ranges in 12.3-15.9 dB. At saturation, the drain efficiency is above 57.4%, and reaches as high as 76.9% at 2.6 GHz. At 9-dB OBO, the drain efficiency of designed DPA maintains at high level across the operating frequency band, ranging from 48.1% to 58.6%. The simulation results show the feasibility of the proposed bandwidth and power back-off enhanced DPA design approach.

IV. Experimental Results

The photo of the fabricated DPA is shown in Fig. 11 and the circuit size is 170 mm $\times$ 100 mm. The DPA was mounted on a heat sink to dissipate the heat during the PA operating. Continuous wave (CW) and modulated signal measurements were conducted. A signal generator was used to provide the proper input signal, and a broadband linear driver was adopted to boost the input power level, and connected between the signal generator and the fabricated DPA. A spectrum analyzer was used to monitor the output signal, and a 30-dB attenuator was inserted before the spectrum analyzer. Several dc voltage suppliers were used to provide desired gate and drain biases.

A. CW Measurement

The measured power sweeping results are shown in Fig. 12, and the frequency sweeping performance is shown in Fig. 13. The target frequency range was from 1.4 to 2.6 GHz in the simulation. During the implementation, the operating bandwidth shifted to the lower frequency a little, and the frequency 2.6 GHz fall outside the valid bandwidth. Thus, the frequency range 1.4-2.5 GHz is presented in the measured

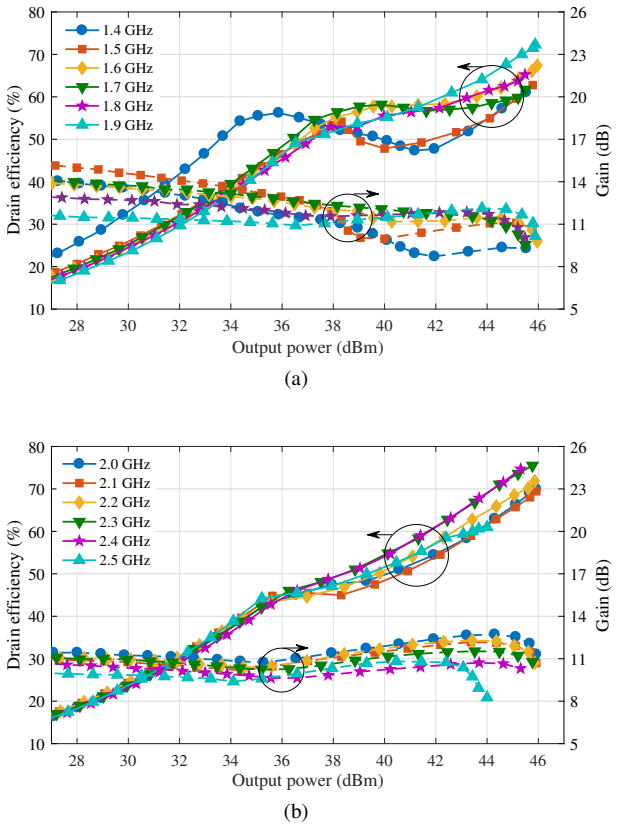

Fig. 12. Measured drain efficiency and gain performance versus output power within the frequency range (a) 1.4-1.9 GHz and (b) 2.0-2.5 GHz.

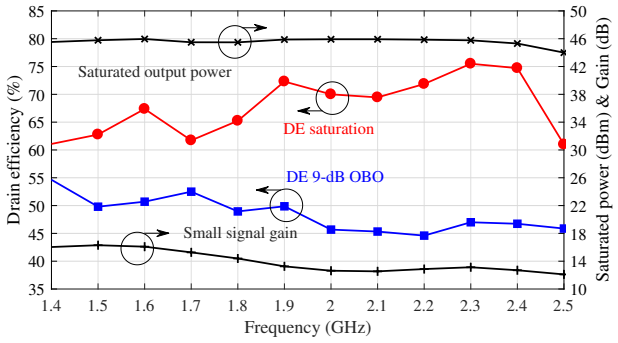

Fig. 13. Measured drain efficiency at power saturation and 9-dB OBO, saturated power and small signal gain performance versus operating frequency.

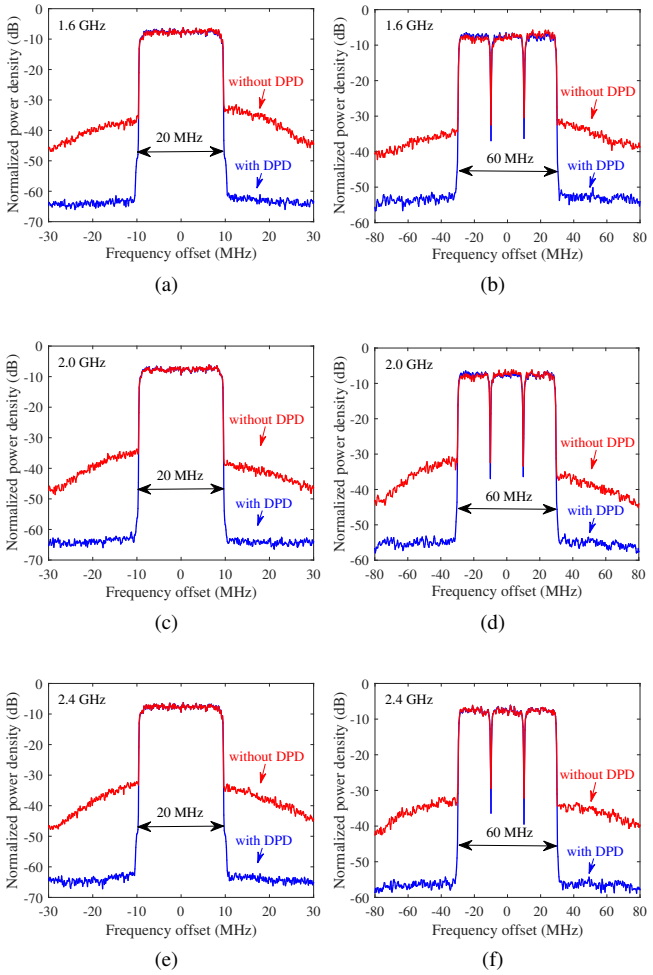

Fig. 14. Spectrum measured under (a) 20 MHz signal at 1.6 GHz (b) 60 MHz signal at 1.6 GHz (c) 20 MHz signal at 2.0 GHz (d) 60 MHz signal at 2.0 GHz (e) 20 MHz signal at 2.4 GHz (f) 60 MHz signal at 2.4 GHz with 9-dB PAPR before and after DPD.

TABLE V
MEASURED ACLR RESULTS WITH AND WITHOUT DPD.

Freq. (GHz)	ACLR (dBc)		ACLR with DPD (dBc)	
	20 MHz	60 MHz	20 MHz	60 MHz
1.6	-29.8	-27.2	-56.3	-45.5
2.0	-30.6	-26	-56.8	-47.4
2.4	-27.3	-25.1	-56.7	-47.4

results, which still corresponds to 56.4% fractional bandwidth. The saturated power inside the bandwidth is above 44 dBm. The maximum output power reaches 45.9 dBm at 2 GHz, and 70% drain efficiency is obtained at this frequency point. The drain efficiency achieves as high as 75.5% at 2.3 GHz, and it maintains over 61% when saturated. At 9-dB OBO, the DPA offers high efficiency across the entire bandwidth. The highest efficiency obtained is 54.6% at 1.4 GHz, and the lowest drain efficiency still reaches 44.5% at 2.2 GHz. The measured small signal gain ranges from 12.1 dB to 16.3 dB. The CW measurement results show that the proposed DPA exhibits the bandwidth and the OBO extension simultaneously.

B. Modulated Signal Measurement

To evaluate the linearity performance, the fabricated DPA was tested with the OFDM signal with 9-dB PAPR. The measurements were carried out at 1.6 GHz, 2.0 GHz and 2.4 GHz respectively, and the signal bandwidths include 20 MHz and 60 MHz.

Digital predistortion (DPD) was applied to linearize the DPA. The measured output signal spectrum is presented in Fig. 14. At 1.6 GHz, the measured adjacent channel leakage ratio (ACLR) is -29.8 dBc with 20 MHz signal and -27.2 dBc with 60 MHz signal. With DPD, the ACLR reaches -56.3 dBc and -45.5 dBc respectively. 54.6% average efficiency and 37.3 dBm

TABLE VI
PERFORMANCE COMPARISON WITH PUBLISHED DPA DESIGNS

Ref. Year	Arch.	Freq. (GHz)	FBW (%)	DE_{sat} (%)	OBO (dB)	DE_{obo} (%)	P_{sat} (dBm)	Gain (dB)	Signal (MHz)	PAPR (dB)	P_{avg} (dBm)	DE_{avg} (%)	ACLR w.o. DPD (dBc)	ACLR with DPD (dBc)
[2] 2015	Asym.	0.75-0.95	23.5	55.4-64.7	6	51.5-63.8	48-48.8	14-15.8	20	9.5	39	44	-26∼-22.2*	-
[3] 2016	Asym.	1.6-2.2	31.6	60-71	10	51-55	46	15-17*	20	9.1	36	50-53*	-32∼-27*	-52∼-48*
[29] 2016	Asym.	1.55-2.35	41	53.8-72.9	8-9	50.4-56.2	43.7-45.2	8.2-10.6	5	8.3	36.5	-	-29.7	-50.3
[24] 2018	CM-DPA	1.6-2.7	51	56-75.3	6	46.5-63.5	43.8-45.2	9.4-11.5	20	7.4	36.5-37.5	41.5-58	-31.7∼-26.5	-50.1
[30] 2018	Sym.	1.35-2.05	41	65-75	9	52-55	41.5-42.4	11.5-14.5*	40	8.9	33	50-53	-33∼-23	-51∼-46.5
[5] 2018	Asym.	1.6-1.9	17.1	78.3-83	10-10.6	46-46.3	43-44.6	9.9-11	5	9.6	32.2	46.5-50*	-34∼-32*	-53.3
[14] 2019	Sym.	1.9-2.4	23	65.2-71.8	8.5-9	44.2-49.7	44.1-44.8	11-14*	20	9	-	-	-31.1∼-26.8	-50.3∼-45
[18] 2019	Sym.	1.1-2.4	74	55.4-68	6	43.8-54.9	43.3-45.4	9.5-11.1	20	6.5	36.5-38.5	42.5-53.5	-31.5∼-26.5	-49
[26] 2020	Sym.	1.4-2.55	58	62-74	6	48-58	41.9-42.2	10-14.8*	6*	6.6	35.5	45-57	-38∼-32*	-56∼-45
This Work	Asym.	1.4-2.5	56.4	61-75.5	9	44.6-54.6	44-45.9	12.1-16.3	20/60	9	36.4-37.3/36.1-37.1	49.9-57.6/47.4-53.5	-30.6∼-27.3/-27.2∼-25.1	-56.7∼-56.3/-47.4∼-45.5

* Read from graphs.

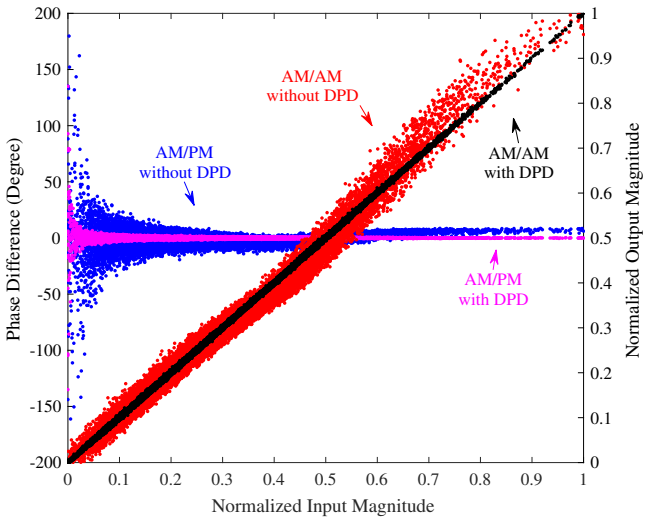

Fig. 15. Measured AM/AM and AM/PM performance with 9-dB PAPR 60 MHz signal at 2.4 GHz with and without DPD.

output power is obtained under 20 MHz signal, and 53.5% efficiency and 37.1 dBm output power is obtained under 60 MHz signal. At 2.0 GHz, the measured ACLR is -30.6 dBc and -26 dBc under 20 MHz and 60 MHz signal respectively, and is further improved to -56.8 dBc and -47.4 dBc after performing DPD. When driven by a 20 MHz signal, the measured average output power is 36.5 dBm with 49.9% average efficiency. For the 60 MHz signal, the measured efficiency is 47.4% with 36.2 dBm output power. At 2.4 GHz, with 20 MHz signal, the measured ACLR is -27.3 dBc, and is improved to -56.7 dBc with DPD. The average efficiency is 50.4% with 36.4 dBm output power. When driven by 60 MHz signal, the measured ACLR is -25.1 dBc, but can reach -47.4 dBc after conducting DPD. The measured efficiency and output power is 47.4% and 36.1 dBm respectively. The ACLR performance before and after DPD is summarized in Table V for comparison. The measured AM/AM and AM/PM with and without DPD is reported in Fig. 15 under 60 MHz 9-dB PAPR signal at 2.4 GHz. In general, when tested with modulated signal with high PAPR, the fabricated DPA shows satisfied linearity performance.

C. Performance Comparison

The performance of the fabricated PA is summarised and compared with other published DPA designs in Table VI. In comparison with other modified DPAs that focus on bandwidth extension, the fabricated design provides comparable bandwidth performance. Most symmetric DPAs show great bandwidth performance but the OBO is limited to 6 dB. When comparing with OBO enhanced designs of both symmetric and asymmetric architectures, the fractional bandwidth of the fabricated DPA is the widest among all. The modulated signal measurement results show the high average efficiency across the bandwidth when compared with other designs, and the measured ACLR for 20 MHz signal is the best among all. When considering bandwidth, OBO and linearity performance all together, the proposed DPA presents well-balanced performance with respect to the mentioned criterion.

V. Conclusion

This paper presented a novel methodology for designing bandwidth and power back-off enhanced Doherty power amplifier. A modified LMN was proposed to provide broadband solutions for a wide range of OBO and current ratio in DPA design. Case studies were conducted to investigate the relationship between the bandwidth and LMN parameters under different OBO levels. Based on the analysis, a series of generalized formulas were derived. The LMN parameters could be easily obtained from the proposed formulas without going through complicated LMN designs. An asymmetric prototype DPA was designed and implemented, achieving 56% fractional bandwidth. The measured drain efficiency at saturation and 9-dB OBO reaches 61%-75.5% and 44.6%-54.6%, respectively. The modified LMN is easy to implement and the design approach is very general. The proposed methodology is thus beneficial in broadband DPA designs.

References

[1] S. Jee, J. Lee, J. Son, S. Kim, C. H. Kim, J. Moon, and B. Kim, "Asymmetric broadband Doherty power amplifier using GaN MMIC for femto-cell base-station," *IEEE Trans. Microw. Theory Tech.*, vol. 63, no. 9, pp. 2802–2810, Sep. 2015.

[2] J. Kwon, M. Seo, H. Lee, J. Gu, J. Ham, K. Hwang, K. Lee, C. Park, and Y. Yang, "Broadband Doherty power amplifier based on asymmetric load matching networks," *IEEE Trans. Circuits Syst. II: Exp. Briefs*, vol. 62, no. 6, pp. 533–537, Jun. 2015.

[3] J. Xia, M. Yang, and A. Zhu, "Improved Doherty amplifier design with minimum phase delay in output matching network for wideband application," *IEEE Microw. Wireless Compon. Lett.*, vol. 26, no. 11, pp. 915–917, Nov. 2016.

[4] H. Jang, P. Roblin, C. Quindroit, Y. Lin, and R. D. Pond, "Asymmetric Doherty power amplifier designed using model-based nonlinear embedding," *IEEE Trans. Microw. Theory Tech.*, vol. 62, no. 12, pp. 3436–3451, Dec. 2014.

[5] X. Y. Zhou, S. Y. Zheng, W. S. Chan, X. Fang, and D. Ho, "Postmatching Doherty power amplifier with extended back-off range based on self-generated harmonic injection," *IEEE Trans. Microw. Theory Tech.*, vol. 66, no. 4, pp. 1951–1963, Apr. 2018.

[6] M. Ozen, K. Andersson, and C. Fager, "Symmetrical Doherty power amplifier with extended efficiency range," *IEEE Trans. Microw. Theory Tech.*, vol. 64, no. 4, pp. 1273–1284, Apr. 2016.

[7] M. R. Hasin and J. Kitchen, "Exploiting phase for extended efficiency range in symmetrical Doherty power amplifiers," *IEEE Trans. Microw. Theory Tech.*, vol. 67, no. 8, pp. 3455–3463, Augest 2019.

[8] H.-Y. Liu, C. Zhai, and K.-K. M. Cheng, "Novel dual-band equal-cell Doherty amplifier design with extended power back-off range," *IEEE Trans. Microw. Theory Tech.*, vol. 68, no. 3, pp. 1012–1021, Mar. 2020.

[9] D. Y. Wu and S. Boumaiza, "A modified Doherty configuration for broadband amplification using symmetrical devices," *IEEE Trans. Microw. Theory Tech.*, vol. 60, no. 10, pp. 3201–3213, Oct. 2012.

[10] D. Gustafsson, C. M. Andersson, and C. Fager, "A modified Doherty power amplifier with extended bandwidth and reconfigurable efficiency," *IEEE Trans. Microw. Theory Tech.*, vol. 61, no. 1, pp. 533–542, Jan. 2013.

[11] R. Giofre, L. Piazzon, P. Colantonio, and F. Giannini, "An ultra-broadband GaN Doherty amplifier with 83% of fractional bandwidth," *IEEE Microw. Wireless Compon. Lett.*, vol. 24, no. 11, pp. 775–777, Nov. 2014.

[12] A. Jundi and S. Boumaiza, "A series-connected-load Doherty power amplifier with push-pull main and auxiliary amplifiers for base station applications," *IEEE Trans. Microw. Theory Tech.*, vol. 68, no. 2, pp. 796–807, Feb. 2020.

[13] X. Fang and K. M. Cheng, "Improving power utilization factor of broadband Doherty amplifier by using bandpass auxiliary transformer," *IEEE Trans. Microw. Theory Tech.*, vol. 63, no. 9, pp. 2811–2820, Sep. 2015.

[14] C. Li, F. You, J. Peng, J. Wang, and M. F. H. S. He, "Co-design of matching sub-networks to realize broadband symmetrical Doherty with configurable back-off region," *IEEE Trans. Circuits Syst. II: Exp. Briefs*, pp. 1–1, 2019.

[15] L. Piazzon, R. GiofrÃ¨, P. Colantonio, and F. Giannini, "A wide-band Doherty architecture with 36% of fractional bandwidth," *IEEE Microw. Wireless Compon. Lett.*, vol. 23, no. 11, pp. 626–628, Nov. 2013.

[16] A. Barakat, M. Thian, V. Fusco, S. Bulja, and L. Guan, "Toward a more generalized Doherty power amplifier design for broadband operation," *IEEE Trans. Microw. Theory Tech.*, vol. 65, no. 3, pp. 846–859, Mar. 2017.

[17] J. J. M. Rubio, V. Camarchia, M. Pirola, and R. Quaglia, "Design of an 87% fractional bandwidth Doherty power amplifier supported by a simplified bandwidth estimation method," *IEEE Trans. Microw. Theory Tech.*, vol. 66, no. 3, pp. 1319–1327, Mar. 2018.

[18] Z. Yang, Y. Yao, M. Li, Y. Jin, T. Li, Z. Dai, F. Tang, and Z. Li, "Bandwidth extension of Doherty power amplifier using complex combining load with noninfinity peaking impedance," *IEEE Trans. Microw. Theory Tech.*, vol. 67, no. 2, pp. 765–777, Feb. 2019.

[19] R. Darraji, D. Bhaskar, T. Sharma, M. Helaoui, P. Mousavi, and F. M. Ghannouchi, "Generalized theory and design methodology of wideband Doherty amplifiers applied to the realization of an octave-bandwidth prototype," *IEEE Trans. Microw. Theory Tech.*, vol. 65, no. 8, pp. 3014–3023, Aug. 2017.

[20] S. Chen, G. Wang, Z. Cheng, and Q. Xue, "A bandwidth enhanced Doherty power amplifier with a compact output combiner," *IEEE Microw. Wireless Compon. Lett.*, vol. 26, no. 6, pp. 434–436, Jun. 2016.

[21] J. Xia, M. Yang, Y. Guo, and A. Zhu, "A broadband high-efficiency Doherty power amplifier with integrated compensating reactance," *IEEE Trans. Microw. Theory Tech.*, vol. 64, no. 7, pp. 2014–2024, Jul. 2016.

[22] J. Pang, S. He, C. Huang, Z. Dai, J. Peng, and F. You, "A post-matching Doherty power amplifier employing low-order impedance inverters for broadband applications," *IEEE Trans. Microw. Theory Tech.*, vol. 63, no. 12, pp. 4061–4071, Dec. 2015.

[23] X. Y. Zhou, S. Y. Zheng, W. S. Chan, S. Chen, and D. Ho, "Broadband efficiency-enhanced mutually coupled harmonic postmatching Doherty power amplifier," *IEEE Trans. Circuits Syst. I, Reg. Papers*, vol. 64, no. 7, pp. 1758–1771, Jul. 2017.

[24] W. Shi, S. He, X. Zhu, B. Song, Z. Zhu, G. Naah, and M. Zhang, "Broadband continuous-mode Doherty power amplifiers with noninfinity peaking impedance," *IEEE Trans. Microw. Theory Tech.*, vol. 66, no. 2, pp. 1034–1046, Feb. 2018.

[25] Y. Li, X. Fang, A. Jundi, H. Huang, and S. Boumaiza, "Two-port network theory-based design method for broadband Class J Doherty amplifiers," *IEEE Access*, vol. 7, pp. 51 028–51 038, Apr. 2019.

[26] H.-Y. Liu, X.-H. Fang, and K.-K. M. Cheng, "Bandwidth enhancement of frequency dispersive Doherty power amplifier," *IEEE Microw. Wireless Compon. Lett.*, vol. 30, no. 2, pp. 185–188, Feb. 2020.

[27] M. Li, J. Pang, Y. Li, and A. Zhu, "Bandwidth enhancement of Doherty power amplifier using modified load modulation network," *IEEE Trans. Circuits Syst. I, Reg. Papers*, vol. 67, no. 6, pp. 1824–1834, Jun. 2020.

[28] J. Pang, Z. Dai, Y. Li, M. Li, and A. Zhu, "Multiband dual-mode Doherty power amplifier employing phase periodic matching network and reciprocal gate bias for 5G applications," *IEEE Trans. Microw. Theory Tech.*, vol. 68, no. 6, pp. 2382–2397, Jun. 2020.

[29] J. Pang, S. He, Z. Dai, C. Huang, J. Peng, and F. You, "Design of a post-matching asymmetric Doherty power amplifier for broadband applications," *IEEE Microw. Wireless Compon. Lett.*, vol. 26, no. 1, pp. 52–54, 2016.

[30] X. Fang, H. Liu, K. M. Cheng, and S. Boumaiza, "Modified Doherty amplifier with extended bandwidth and back-off power range using optimized peak combining current ratio," *IEEE Trans. Microw. Theory Tech.*, vol. 66, no. 12, pp. 5347–5357, Dec. 2018.

[31] C. R. Chappidi, X. Wu, and K. Sengupta, "Simultaneously broadband and back-off efficient mm-Wave PAs: A multi-port network synthesis approach," *IEEE J. Solid-State Circuits*, vol. 53, no. 9, pp. 2543–2559, Sep. 2018.

[32] A. Barthwal, K. Rawat, and S. K. Koul, "A design strategy for bandwidth enhancement in three-stage Doherty power amplifier with extended dynamic range," *IEEE Trans. Microw. Theory Techn.*, vol. 66, no. 2, pp. 1024–1033, Feb. 2018.

[33] J. Xia, W. Chen, F. Meng, C. Yu, and X. Zhu, "Improved three-stage Doherty amplifier design with impedance compensation in load

combiner for broadband applications," *IEEE Trans. Microw. Theory Tech.*, vol. 67, no. 2, pp. 778–786, Feb. 2019.

[34] J. Pang, Y. Li, C. Chu, J. Peng, X. Y. Zhou, and A. Zhu, "Extend high efficiency range of Doherty power amplifier by modifying characteristic impedance of transmission lines in load modulation network," in *IEEE MTT-S Int. Microw. Symp. Dig.*, IEEE, Aug. 2020, pp. 1–4.

[35] P. J. Tasker and J. Benedikt, "Waveform inspired models and the harmonic balance emulator," *IEEE Microw. Mag.*, vol. 12, no. 2, pp. 38–54, Apr. 2011.

[36] K. Chen and D. Peroulis, "Design of highly efficient broadband Class-E power amplifier using synthesized low-pass matching networks," *IEEE Trans. Microw. Theory Tech.*, vol. 59, no. 12, pp. 3162–3173, Dec. 2011.

Yang Xu (Graduate Student Member, IEEE) received the B.E. and M.E. degree in electronic engineering from Harbin Institute of Technology (HIT), Harbin, China in 2013 and 2015, respectively. She is currently pursuing the Ph.D. degree at University College Dublin (UCD), Dublin, Ireland.

She is currently with the RF and Microwave Research Group, UCD. Her research interests include highly efficient broadband power amplifiers and MMIC power amplifiers in RF/microwave and millimeter-wave applications for 5G and beyond.

Jingzhou Pang (Member, IEEE) received the B.S. degree in electrical engineering and Ph. D. degree in circuits and systems from University of Electronic Science and Technology of China (UESTC), Chengdu, China, in 2010 and 2016, respectively. From December 2016 to July 2018, he was with Huawei Technologies Company Ltd., Chengdu, China, where he was an engineer in charge of the research and development of 5G high efficiency power amplifiers and transmitters. From July 2018 to August 2020, he was with the RF and Microwave Research Group at University College Dublin (UCD), Dubin, Ireland, where he was a research fellow in charge of the research of novel broadband transmitter architectures and RF/Microwave/mm-wave MMIC power amplifiers. He is currently an associate professor with the School of Microelectronics and Communication Engineering, Chongqing University, Chongqing, China. His research interests include broadband high-efficiency power amplifier systems, bandwidth extension techniques for high-efficiency transmitters and MMIC power amplifier design for RF/microwave and millimeter-wave applications.

Dr. Pang was a recipient of the EDGE Marie Sklodowska-Curie Individual Fellowship. He was a recipient of third Place Award of the High Efficiency Power Amplifier Student Design Competition, IEEE Microwave Theory and Techniques Society (IEEE MTT-S) International Microwave Symposium (IMS) in 2013.

Xiaoyu Wang (Graduate Student Member, IEEE) received the B.E. degree in information engineering from Southeast University, Nanjing, China, in 2015. She is currently pursuing the Ph.D. degree at University College Dublin (UCD), Dublin, Ireland.

She is currently with the RF and Microwave Research Group, UCD. Her current research focuses on digital predistortion for RF power amplifiers, with a particular emphasis on applications to multiple-input multiple-output (MIMO) systems.

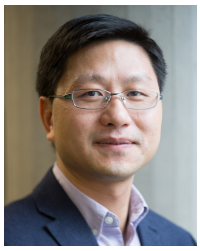

Anding Zhu (Senior Member, IEEE) received the Ph.D. degree in electronic engineering from University College Dublin (UCD), Dublin, Ireland, in 2004.

He is currently a Professor with the School of Electrical and Electronic Engineering, UCD. His research interests include high-frequency nonlinear system modeling and device characterization techniques, high-efficiency power amplifier design, wireless transmitter architectures, digital signal processing, and nonlinear system identification algorithms. He has published more than 150 peer-reviewed journal and conference articles.

Prof. Zhu is an elected member of MTT-S AdCom, the Chair of the Electronic Information Committee and the Vice Chair of the Publications Committee. He is also the Chair of the MTT-S Microwave High-Power Techniques Committee. He served as the Secretary of MTT-S AdCom in 2018. He was the General Chair of the 2018 IEEE MTT-S International Microwave Workshop Series on 5G Hardware and System Technologies (IMWS-5G) and a Guest Editor of the IEEE TRANSACTIONS ON MICROWAVE THEORY AND TECHNIQUES on 5G Hardware and System Technologies. He is currently an Associate Editor of the IEEE Microwave Magazine and a Track Editor of the IEEE TRANSACTIONS ON MICROWAVE THEORY AND TECHNIQUES.